Modular Vector Control of Multi-Three-Phase Permanent Magnet Synchronous Motors

Sandro Rubino, *Member, IEEE*, Obrad Dordevic, *Member, IEEE*,
Radu Bojoi, *Fellow, IEEE* and Emil Levi, *Fellow, IEEE*

***Abstract*—Recent developments in power electronics are making the multiphase machines a competitive alternative to conventional three-phase counterparts. Due to their fault-tolerant features, multiphase drives represent a robust technology in high power/high current, safety-critical applications. Besides, their introduction into transportation electrification is gaining on importance. Among the multiphase solutions, the multi-three-phase machines are receiving a lot of the attention by the industry since they use the well-consolidated three-phase technology, thus reducing the design time and also the cost. Therefore, this paper proposes a modular vector control scheme for multi-three-phase permanent magnet synchronous motors. The proposed solution uses a modular modeling approach for the independent and decoupled torque control of each three-phase unit, allowing the implementation of torque-sharing strategies among the three-phase sets of the machine. The developed modular control has been validated on a nine-phase permanent magnet machine.**

***Index Terms*—Multiphase machines, multi-three-phase drives, permanent magnet synchronous motors, modular current control, torque- and current- sharing.**

I. Introduction

In recent years, transportation electrification and the energy production from renewables have become strategic sectors that are requiring new electrical technologies based on robust and reliable solutions [1].

Thanks to the recent advancements in power electronics, the multiphase systems (number of phases higher than three) nowadays represent a competitive solution for safety-critical, high power/high current applications [2]–[4]. Compared to the three-phase solution, the increase of the phase number allows the reduction of the phase current without increasing the voltage per phase [5], facilitating the use of fast electronic devices. In this way, it is possible to get high dynamic performance also in high-power systems, where the dynamic performance is typically limited by the use of slow, high current devices.

Among all possible multiphase structures, the multi-three-phase systems (Fig. 1) are an attractive solution for industry, as the three-phase technologies are well-consolidated and provide high performance at a reduced cost [6], [7].

Manuscript received May 08, 2020; revised July 29, 2020, and September 03, 2020; accepted September 06, 2020.

Sandro Rubino and Radu Bojoi are with the Dipartimento Energia "G. Ferraris", Politecnico di Torino, Torino, 10129, Italy (e-mail: sandro.rubino@polito.it; radu.bojoi@polito.it).

Obrad Dordevic and Emil Levi are with the Faculty of Engineering and Technology, Liverpool John Moores University, Liverpool L3 3AF, U.K., (e-mail: o.dordevic@ljmu.ac.uk; e.levi@ljmu.ac.uk).

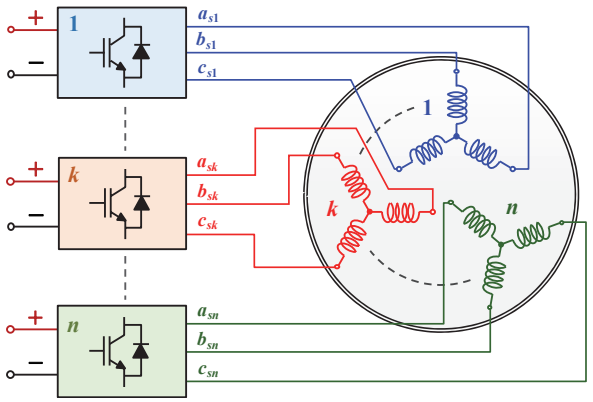

Fig. 1. Generic multi-three-phase drive topology.

A multi-three-phase electrical machine has a stator consisting of independent three-phase windings with isolated neutral points that are supplied by three-phase inverter units [8]–[10]. In this way, the power converter can be designed as multiple three-phase power modules (Fig. 1) with a relevant saving in terms of size, cost, and development time [6], [7]. In case of a fault of the power module, the faulted three-phase unit (winding plus converter) is simply disconnected from the dc power supply, thus yielding a straightforward post-fault reconfiguration [11].

The multiphase machines are divided into symmetrical or asymmetrical machines, according to the electrical displacement γ between the magnetic axes of two adjacent stator phases [6]. When the number of phases n_{ph} is multiple of three and an even number (e.g., $n_{ph} = 6, 12$), the machine is usually designed as asymmetrical, with a spatial displacement γ between the first phases of two consecutive sets equal to $180/n_{ph}$ electrical degrees: 30 electrical degrees for a six-phase machine, 15 electrical degrees for a twelve-phase machine, etc.

To reduce the machine cost, off-the-shelf stator cores designed for three-phase machines are often employed [12]. However, this approach can lead to atypical configurations of the stator winding, for which the spatial displacement γ between the first phases of two consecutive sets is different from the conventional value of $180/n_{ph}$ electrical degrees. Unfortunately, such configurations of the stator winding lead to many complications for machine modeling and control. As an example, the most employed method for multiphase machines modeling, the vector space decomposition (VSD) approach [3], [13], [14], currently does not provide solutions for dealing with such winding configurations, as demonstrated in [15].

The approach that solves the problem is the multi-stator (MS) modeling approach [6], [16] that simply considers the machine

as multiple three-phase stator sets interacting with each other and with the rotor, without any limitations regarding the configuration of the stator winding. This approach highlights the contributions to the machine flux and torque provided by each three-phase winding set, and it is particularly suitable for the implementation of modular control schemes of each three-phase unit [17], [18]. This feature is useful in the "series-parallel" configurations, where power-sharing among the units is often performed [4], [17], [19], [20].

Besides the capability to deal with any multi-three-phase configuration of the stator winding, the MS approach allows the easy reconfiguration of the MS-based control schemes after an open-winding fault event [6], [8]. However, MS modeling is characterized by strong magnetic couplings among the three-phase sets [16]. Indeed, the MS approach maps the energy conversion into n (d,q) subspaces, where n is the number of the three-phase sets of the machine [6]. As demonstrated in [10], the coupling among the sets can cause instability of the MS-based control schemes, making necessary the limitation of their dynamic performance. Besides, this issue gets worse for multi-three-phase machines with ($n \geq 3$) [17], [21].

Therefore, the goal of this work is to propose an MS-based modular vector control scheme for multi-three-phase permanent magnet synchronous machines (PMSM). Compared to the solutions reported in the literature, the contributions of the paper are:

1) A modular vector control scheme that can be implemented on any multi-three-phase PMSM, regardless of the configuration of the stator winding that may lead to different parameters of the sets.
2) A straightforward decoupling algorithm for MS-based control schemes that allow an independent and decoupled control of each three-phase set.
3) The removal of all the limitations that prevent instability of the MS-approach, allowing the machine control to get the best dynamic performance using a simple drive scheme suitable for the industrial applications.

More specifically, the proposed solution performs a decoupling action among the voltages of the winding sets, avoiding dangerous interactions that can cause the instability of the modular vector control scheme. The experimental validation has been carried out on a nine-phase PMSM that uses an atypical triple-three-phase configuration of the stator winding, with 15° electrical between two consecutive three-phase sets (instead of 20° for asymmetrical nine-phase machines or 40° for symmetrical ones). The paper builds on [22] and brings in added value by including:

- An extended machine modeling and a decoupling algorithm valid for both isotropic and anisotropic multi-three-phase PMSMs.
- Additional experimental validation for torque sharing operation in healthy and faulty conditions, demonstrating the fault ride-through capability.

The paper is organized as follows. Section II contains an exhaustive analysis of the MS modeling of multi-three-phase PMSMs. The proposed control solution is described in Section III, whereas the experimental validation is provided in Section IV. Section V reports the conclusions.

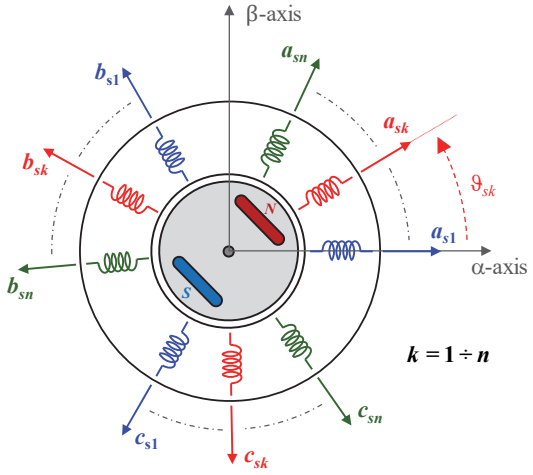

Fig. 2. Generic configuration of a multi-three-phase PMSM: angle displacement of the magnetic axes in one electrical revolution.

II. MS Modeling of a Multi-Three-Phase PMSM

The MS approach considers a multi-three-phase machine as multiple three-phase sets operating in parallel. In this way, the electromechanical modularity is preserved since each three-phase set is independently treated.

In the following, a PMSM with a sinusoidal distribution of the stator windings is assumed; these interact with each other and the permanent magnets (PM) only through the spatial-fundamental component of the airgap field, neglecting the effects of the high order harmonics. The numbers of pole pairs p and three-phase winding sets n are considered arbitrary.

According to the MS modeling, for each generic set k (k=1÷n), the general Clarke transformation is applied [23], using the following amplitude-invariant form:

$$[C_k] = \frac{2}{3} \cdot \begin{bmatrix} \cos(\vartheta_{sk}) & \cos(\vartheta_{sk} + 2\pi/3) & \cos(\vartheta_{sk} + 4\pi/3) \\ \sin(\vartheta_{sk}) & \sin(\vartheta_{sk} + 2\pi/3) & \sin(\vartheta_{sk} + 4\pi/3) \\ 1/2 & 1/2 & 1/2 \end{bmatrix} \quad (1)$$

where ϑ_{sk} stands for the characteristic angle of the considered set. This angle is defined as the position of the first phase (a_{sk}-phase) of the set k to the α-axis; the latter is conventionally made coincident with the first phase of the first set (a_{s1}-phase), as shown in Fig. 2. In this way, n overlapped stationary models (αβ0) are obtained. No constraints on the values of the characteristic angles are assumed, thus dealing with the most generic case.

The electromagnetic model of the machine in (d,q) coordinates is considered. The d-axis position is assumed coincident with that of the PM flux linkage vector, as schematically shown in Fig. 3. The magnetic saturation and iron losses are not considered.

A. Electromagnetic Model in (d, q) Coordinates

The application of the MS approach on a generic multi-three-phase PMSM leads to n electromagnetic equation systems. For each generic set k, the (d,q) electric model is computed as:

$$\bar{v}_{sk,dq} = R_{sk} \cdot \bar{i}_{sk,dq} + \frac{d}{dt}\bar{\lambda}_{sk,dq} + J \cdot \omega_r \cdot \bar{\lambda}_{sk,dq} \quad (2)$$

where $\bar{x}_{sk,dq}=[x_{sk,d} \quad x_{sk,q}]^t$ is a k-set stator vector that can assume the meaning of voltage v, current i, and flux linkage λ. Each generic set k is characterized by its own resistance R_{sk}.

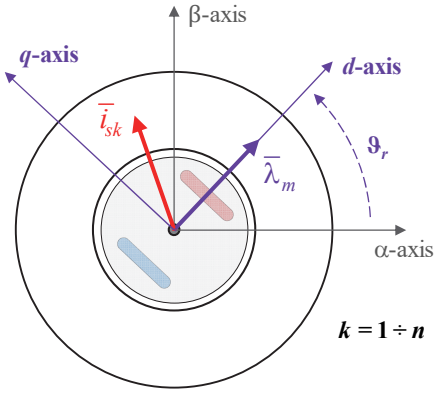

Fig. 3. (*d*,*q*) frame for a multi-three-phase PMSM: configuration of the magnetic axes in one electrical revolution.

The rotor electrical position ϑ_r, corresponding to that of the *d*-axis, is defined as $\vartheta_r = p \cdot \vartheta_m$, where ϑ_m is the rotor mechanical position. Therefore, by finding the time derivative, the rotor electric speed ω_r is computed as $\omega_r = p \cdot \omega_m$, where ω_m is the rotor mechanical speed. The variable J is the operator $\begin{bmatrix} 0 & -1 \\ 1 & 0 \end{bmatrix}$.

Regarding the magnetic model of the machine, for each set k the following (*d*,*q*) equation is computed:

$$\bar{\lambda}_{sk,dq} = L_{lsk} \cdot \bar{i}_{sk,dq} + \begin{bmatrix} M_d & 0 \\ 0 & M_q \end{bmatrix} \cdot \sum_{z=1}^{n} \bar{i}_{sz,dq} + \begin{bmatrix} \lambda_m \\ 0 \end{bmatrix} \tag{3}$$

where M_d and M_q represent the magnetizing inductances in the *d*-axis and *q*-axis, respectively. It is noted how the flux linkage of each set also depends on the (*d*,*q*) currents of the others (z=1÷n), leading to a significant magnetic coupling. Similarly to the electric model, it is assumed that each set is characterized by its own leakage inductance L_{lsk}. Therefore, unlike the VSD modeling, it is noted how the MS approach allows consideration of different values of the stator parameters (R_{sk}, L_{lsk}) in the sets. Finally, λ_m represents the amplitude of the PM flux linkage. Since the sets share the same number of winding turns, the amplitude of the PM flux linkage is univocal.

The electromagnetic torque of each set k is computed through the power balance of the machine, leading to:

$$T = \sum_{k=1}^{n} T_k = \frac{3}{2} \cdot p \cdot \sum_{k=1}^{n} \left(\bar{\lambda}_{sk,dq} \wedge \bar{i}_{sk,dq} \right) \tag{4}$$

where T_k is the *k*-set torque contribution, T is the overall electromagnetic torque, while $\wedge$ stands for the operator of outer product. It is noted how the machine torque is the sum of the contributions of the n sets that interact with the rotor. Therefore, the modularity of the MS approach is demonstrated. Indeed, each three-phase set is characterized by its electromagnetic- and torque- equations, as confirmed by Fig. 4, where the steady-state equivalent (*d*,*q*) circuit of the machine is depicted.

B. State-Space Model in (*d*, *q*) Coordinates

The computation of the MS electromagnetic model demonstrates how the coupling among the sets can have a massive impact on the control of the machine currents. Therefore, the design of a modular control scheme requires the computation of the state-space model associated with each set.

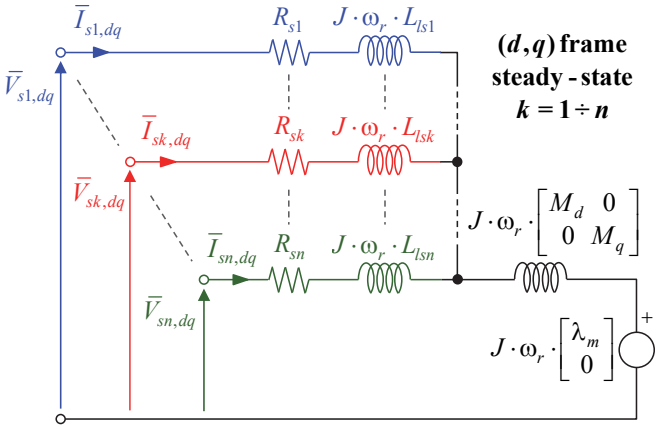

Fig. 4. Steady-state equivalent (*d*,*q*) circuit of a generic multi-three-phase PMSM.

This operation is easy to perform when considering the VSD machine model [19]. The VSD transformation performs a harmonic decoupling of the machine model in phase coordinates [13], [15]. The energy conversion is concentrated in an average subspace, having the meaning of the time-fundamental model of the machine. Therefore, the state-space model of such a subspace can be found easily in the literature, being identical to that of a three-phase machine [23]. However, the unbalances among the sets in terms of both flux and torque productions are expressed through the harmonic subspaces [9], [19], [24], making the VSD modeling less straightforward for the implementation of modular control schemes.

Unlike the VSD modeling, the MS approach delivers a dedicated electromagnetic equation system (2)-(4) for each set of the machine, highlighting its flux and torque productions. Nevertheless, the magnetic coupling among the sets makes the computation of the state-space models associated with them difficult. Except for the induction machine [17], [25], there is no report of solutions for a multi-three-phase PMSM with an arbitrary number of sets, hindering the development of efficient decoupling algorithms for MS-based control schemes.

Starting from the electromagnetic equation system of each set (2)-(4), the state-space MS model in (*d*,*q*) coordinates of a generic multi-three-phase PMSM is derived next. Preliminary auxiliary variables are defined as:

$$w_{d,k} = M_d \cdot \frac{x_{f,k}}{L_{lsk}} \qquad c_{d,k} = M_d \cdot \sum_{z=1, z \neq k}^{n} \frac{x_{f,z}}{L_{lsz}} \tag{5}$$

$$w_{q,k} = M_q \cdot \frac{x_{f,k}}{L_{lsk}} \qquad c_{q,k} = M_q \cdot \sum_{z=1, z \neq k}^{n} \frac{x_{f,z}}{L_{lsz}} \tag{6}$$

making the interpretation of the state-space equations easier. The variable $x_{f,k}$ stands for the logic status of the generic set k (0-OFF/1-ON), allowing adaptation of the state-space models of the healthy sets after an open-winding fault event. Finally, since this work proposes a modular control scheme, the (*d*,*q*) currents of each set are considered as state-space variables.

After performing the mathematical manipulations shown in the Appendix, the computation of the state-space model associated with a generic set k (k=1÷n) yields:

$$\begin{cases} L_{d,k}\cdot\dfrac{d}{dt}i_{sk,d} = X_{dd,k}\cdot i_{sk,d} + X_{dq,k}\cdot i_{sk,q} + \ldots \\ \quad \ldots + \displaystyle\sum_{z=1,z\neq k}^{n}\left(Y_{dd,z}\cdot i_{sz,d} + Y_{dq,z}\cdot i_{sz,q}\right) + F_{k,d} \\ L_{q,k}\cdot\dfrac{d}{dt}i_{sk,q} = X_{qd,k}\cdot i_{sk,d} + X_{qq,k}\cdot i_{sk,q} + \ldots \\ \quad \ldots + \displaystyle\sum_{z=1,z\neq k}^{n}\left(Y_{qd,z}\cdot i_{sz,d} + Y_{qq,z}\cdot i_{sz,q}\right) - \omega_r\cdot\lambda_m + F_{k,q} \end{cases} \quad (7)$$

Expressions in (7) lead to the following considerations:

1) Each set k is characterized by its own (d,q) inductances, values of which are computed as:

$$L_{d,k} = M_d + L_{lsk}\cdot\left(1+c_{d,k}\right) \qquad L_{q,k} = M_q + L_{lsk}\cdot\left(1+c_{q,k}\right) \quad (8)$$

2) The self-coupling of each set k, consisting of the influence of the k-set currents on their time-derivatives, depends on the following parameters:

$$X_{dd,k} = -R_{sk}\cdot\left(1+c_{d,k}\right) \qquad X_{dq,k} = \omega_r\cdot\left[M_q + L_{lsk}\cdot\left(1+c_{d,k}\right)\right]$$
$$X_{qd,k} = -\omega_r\cdot\left[M_d + L_{lsk}\cdot\left(1+c_{q,k}\right)\right] \qquad X_{qq,k} = -R_{sk}\cdot\left(1+c_{q,k}\right) \quad (9)$$

3) Each mutual coupling of the set k, consisting of the influence of the z-set currents (z=1÷n, $z\neq k$) on the time-derivatives of the k-set currents, depends on the following parameters:

$$Y_{dd,z} = R_{sz}\cdot w_{d,z} \qquad Y_{qq,z} = R_{sz}\cdot w_{q,z}$$
$$Y_{dq,z} = Y_{qd,z} = \omega_r\cdot\left(M_q - M_d\right) \quad (10)$$

4) Like for a three-phase machine, the back-electromotive forces (emf) caused by the PM ($\omega_r\cdot\lambda_m$) act only on the q-axis, regardless of the considered set.

5) The time-derivatives of the k-set currents can be controlled through the forcing terms $F_{k,d}$ and $F_{k,q}$. These variables consist of linear combinations of the (d,q) voltages belonging to sets as:

$$F_{k,d} = \left(1+c_{d,k}\right)\cdot v_{sk,d} - \sum_{z=1,z\neq k}^{n}\left(w_{d,z}\cdot v_{sz,d}\right)$$
$$F_{k,q} = \left(1+c_{q,k}\right)\cdot v_{sk,q} - \sum_{z=1,z\neq k}^{n}\left(w_{q,z}\cdot v_{sz,q}\right) \quad (11)$$

According to (7)-(11), the currents of each set also depend on the voltages applied to the others. This 'voltage coupling' among the sets represents the leading cause of instability of the MS-based control schemes [10], requiring the implementation of specific decoupling algorithms.

Therefore, starting from the machine MS state-space model (7), the design of a proper decoupling algorithm can be performed. In this way, all the limitations that avoid instability of MS-based control schemes can be removed, allowing the control of the currents of each set directly, and with high dynamic performance.

III. Modular Current Vector Control

The proposed control solution is implemented in rotating (d,q) coordinates, allowing straightforward torque sharing operation among the sets. Indeed, the choice of the rotor (d,q) frame makes the state-space model of the machine totally independent of the load-angle values of the sets. In this way, significant simplifications on the design of the decoupling algorithm are obtained [17]. As noted, the main advantage of the modularity consists of the possibility to deal with atypical configurations of the machine winding. Also, any asymmetries between the stator parameters of the sets can be easily managed.

The modular control current scheme is shown in Fig. 5. One can see how each unit k is controlled directly, and it receives the (d,q) currents references $i_{sk,dq}^{*}$ from an external drive scheme. Besides, the current vector control (CVC) of each unit k is characterized by its amplitude limit of the phase-currents $I_{sk,max}$, thus dealing with the most generic case. The output of each CVC scheme consists of the reference forcing terms $F_{k,d}^{*}$ and $F_{k,q}^{*}$, having the same meaning as in (11). Finally, after the application of the proposed decoupling algorithm (Fig. 5), the duty-cycles $[\delta^{*}_{k,abc}]$ of each VSI unit k (k=1÷n) are computed, taking into account its value of the dc-link voltage $v_{dc,k}$. A detailed description of the proposed solution is given next.

A. Drive Scheme

The k-unit reference (d,q) currents can be generated in many ways, depending on the configuration of the drive scheme. In this work, the solution shown in Fig. 6 is proposed. The primary input of the machine control scheme is the overall reference torque T^{*}. This command can consist of the sum of units' reference torques T_k^{*} (k=1÷n), each of these provided by an outer control loop. Such configuration is typical of the 'series/parallel' systems proposed for wind energy production [9], [20].

Alternatively, the overall reference torque can be provided by a speed controller, thus performing the closed-loop speed operation of the machine. Both options are reported in Fig. 6, and they can be selected through the selector s_T. In the following, the superscript * denotes a reference variable, distinguishing it from those measured.

Once the overall reference torque is obtained, the optimal (d,q) currents of each set ($i_{s,d}^{opt}$,$i_{s,q}^{opt}$) are computed, using the maximum-torque per ampere (MTPA) profiles of the machine [26]. In this way, the better exploitation of the machine currents is obtained. The MTPA profiles consider a balanced operation of the sets, and they require an accurate mapping of the machine, as for the three-phase PMSM drives [27]. In this way, the magnetic saturation can also be considered.

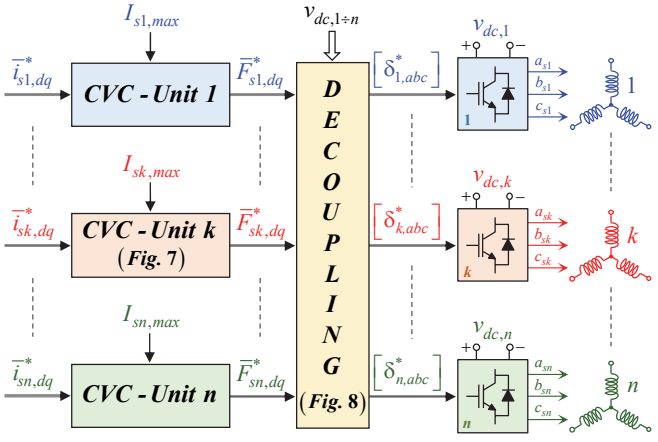

Fig. 5. Modular current vector control scheme.

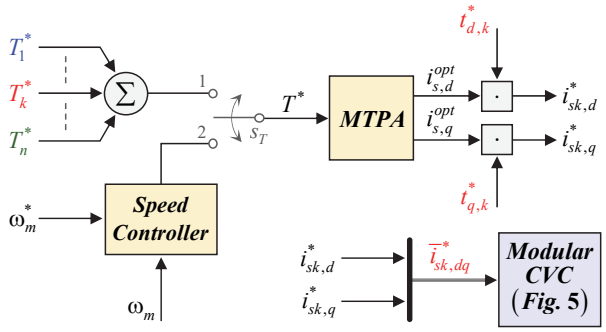

Fig. 6. Proposed drive scheme.

If a surface-mount configuration of the PM is considered, the magnetizing (d,q) inductances are identical to each other. In this specific case, the optimal (d,q) currents of the sets are computed as:

$$M_d = M_q \;\Rightarrow\; i_{s,d}^{opt} = 0 \;,\; i_{s,q}^{opt} = 2 \cdot T^* \Big/ \left(3 \cdot p \cdot n \cdot \tilde{\lambda}_m\right) \quad (12)$$

where superscript ˜ stands for an estimated parameter.

Finally, the reference (d,q) currents of a generic set k are computed by applying the torque-sharing coefficients ($t_{d,k}^*$,$t_{q,k}^*$), as shown in Fig. 6. Such coefficients must be defined to satisfy the torque reference T_k^* of each set, in both healthy and faulty (open-winding) conditions. Besides, in the case of magnetic saturation, or different values of the magnetizing (d,q) inductances, the computation of torque-sharing coefficients must consider the genuine torque-to-currents relationships of the machine. This issue is not considered here, as it is beyond the purpose of this work. If considering the same conditions under which (12) has been computed, the torque-sharing coefficients of a generic set k are defined as:

$$t_{d,k}^* = 0 \quad , \quad t_{q,k}^* = x_{f,k} \cdot T_k^* \Big/ T^* \quad , \quad \sum_{k=1}^{n} t_{q,k}^* = 1 \qquad (13)$$

Once the reference (d,q) currents of each set are computed, the modular CVC (Fig. 5) is performed.

B. Modular Current Control

The CVC scheme of a generic unit k is shown in Fig. 7. According to the d-axis reference current, and the amplitude limit of the k-unit phase-currents $I_{sk,max}$, the q-axis reference current can be limited, thus avoiding the overcurrent operation of the unit. Concerning the feedback currents of the unit ($i_{sk,d}$, $i_{sk,q}$), these are computed by applying the k-unit Clarke transformation (1), followed by that rotational, on the measured values of the k-unit phase-currents (Fig. 7).

The k-unit CVC is performed using standard proportional-integral (PI) controllers. The current controllers must be designed to consider the voltage coupling among the sets. According to (7)-(11), the (d,q) currents of each set also depend on the (d,q) voltages of the other units. Therefore, the outputs of the k-unit controllers ($F_{k,d}^*$, $F_{k,q}^*$) must be considered as a reference combination of the (d,q) voltages of all units, with the same meaning as in (11). If the outputs of the k-unit controllers are set as reference voltages of the unit, significant conflicts with the controllers of the other units arise, leading to the potential instability of the modular CVC [10].

Regarding the design of the controllers' gains, it is possible to adopt the same tuning procedures as for the CVC of three-phase PMSMs.

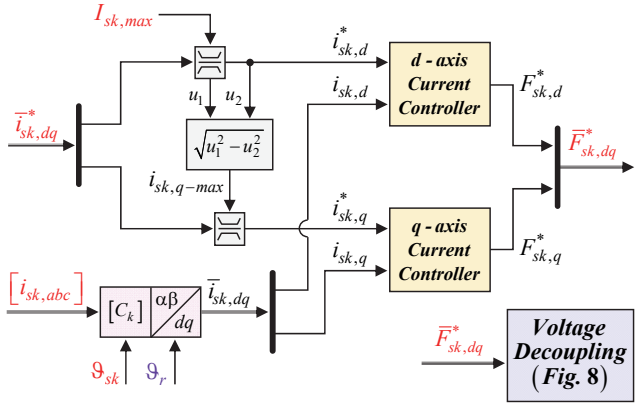

Fig. 7. CVC scheme of each unit k.

In detail, for each set, the equivalent parameters of inductance (8) and resistance (9) must be considered. Therefore, if asymmetries among the parameters of the sets occur, different values of the controllers' gains among the units are obtained, especially for a given bandwidth of the control loops. Finally, the feed-forward compensation of mutual couplings among the sets (10) is recommended, thus increasing the dynamic performance of the CVC.

C. Voltage Decoupling Algorithm

The outputs of each CVC scheme correspond to specific reference combinations ($F_{k,d}^*$, $F_{k,q}^*$) of the (d,q) voltages belonging to all units. Therefore, a decoupling algorithm to extrapolate the reference voltages of each unit ($v_{sk,d}^*$, $v_{sk,q}^*$) from the reference combinations provided by all CVC schemes ($F_{k,d}^*$, $F_{k,q}^*$, k=1÷n) must be implemented (Fig. 8). Based on (11), the outputs of the k-unit controllers can be expressed as:

$$\begin{aligned} F_{k,d}^* &= (1+c_{d,k}) \cdot v_{sk,d}^* - \sum_{z=1,z\neq k}^{n} \left(w_{d,z} \cdot v_{sz,d}^*\right) \\ F_{k,q}^* &= (1+c_{q,k}) \cdot v_{sk,q}^* - \sum_{z=1,z\neq k}^{n} \left(w_{q,z} \cdot v_{sz,q}^*\right) \end{aligned} \qquad (14)$$

Therefore, the proposed decoupling algorithm consists of inverting the expressions (14). According to the Appendix, the following solutions are computed:

$$\begin{aligned} v_{sk,d}^* &= \left(1+\sum_{z=1}^{n} \tilde{w}_{d,z}\right)^{-1} \cdot \left[F_{k,d}^* + \sum_{z=1}^{n}\left(\tilde{w}_{d,z} \cdot F_{z,d}^*\right)\right] \\ v_{sk,q}^* &= \left(1+\sum_{z=1}^{n} \tilde{w}_{q,z}\right)^{-1} \cdot \left[F_{k,q}^* + \sum_{z=1}^{n}\left(\tilde{w}_{q,z} \cdot F_{z,q}^*\right)\right] \end{aligned} \qquad (15)$$

Such solutions guarantee the satisfaction of the reference combinations (14) required by each CVC scheme (Fig. 5), thus ensuring the control of each set with high performance. Finally, the q-axis voltage component of each unit could be limited to respect the amplitude limit of the phase-voltages $v_{sk,max}$, as shown in Fig. 8. Such a limit depends on both the dc-link voltage of the unit $v_{dc,k}$ and the adopted pulse-width modulation technique (PWM).

D. Pulse-Width Modulation

Since each winding set is fed by a dedicated VSI (Fig. 1), independent PWM modulators are employed. In this way, the well-known three-phase modulation techniques [28] can still be implemented, as shown in Fig. 9.

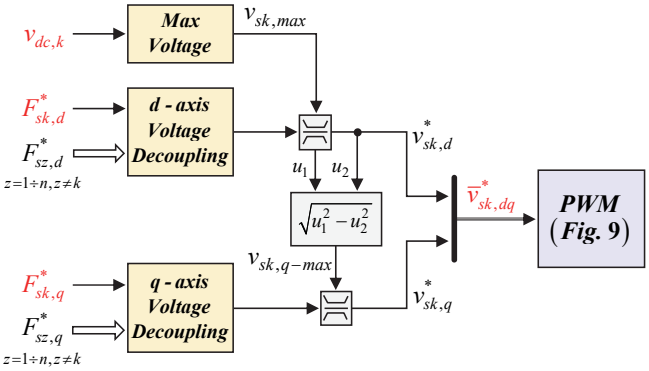

Fig. 8. Voltage decoupling of each unit *k*.

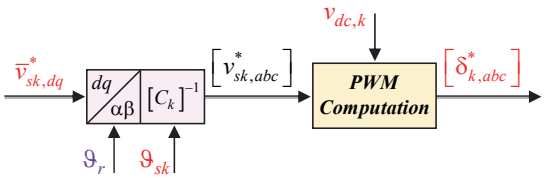

Fig. 9. PWM modulation of each unit *k*.

Therefore, the amplitude limit of the *k*-unit phase-voltages is computed as $v_{sk,max} = v_{dc,k} / \sqrt{3}$, allowing the maximum exploitation of the *k*-unit dc bus. In this work, the duty-cycle commands of each unit $[\delta^*_{k,abc}]$ are computed using the 'Min-Max' modulation [28].

IV. Experimental Validation

The proposed control solution has been validated on a nine-phase surface-mount PMSM using a triple-three-phase stator winding configuration.

The machine has been obtained from a three-phase PMSM with 6 poles and 36 stator slots, thus reducing cost and design time. However, due to the high number of both rotor poles and stator phases, the overall number of slots has not been sufficient to make a regular winding configuration [15]. As a result, the spatial displacement γ between the first phases of two consecutive sets is 15 electrical degrees instead of the conventional values of 20° or 40° electrical as shown in Fig. 10.

Furthermore, since the angular electrical displacement between two consecutive slots is 30° degrees, the second set (a_{s2},b_{s2},c_{s2}) has been made by splitting each phase winding between two adjacent slots, as shown in Fig. 11. Therefore, despite the same number of winding turns, the second set has a stator leakage inductance that is close to half of one of the other sets. Conversely, the stator resistance is about the same for all sets, as shown in Table I, which lists the main machine parameters.

A. Test Rig

The machine has been mounted on a test rig for validation purposes. The rotor shaft has been coupled to a dc machine acting as an active mechanical load (Fig. 12). Due to the mechanical limitations of the test rig, the maximum speed has been limited at ± 1500 rpm. The rotor mechanical position has been measured with an incremental encoder having a resolution of 1000 pulses/rev.

The power converter consists of custom-made VSIs, based on the insulated-gate bipolar transistor (IGBT) modules

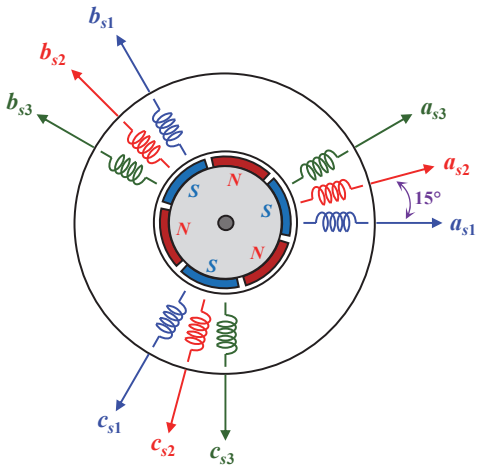

Fig. 10. Nine-phase surface-mount PMSM using an atypical triple-three-phase stator winding configuration (6 poles).

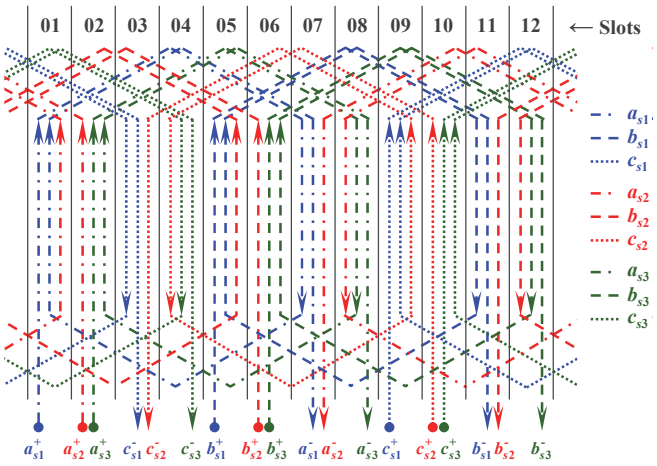

Fig. 11. Stator winding configuration for one pole-pair of the machine (two parallel paths for each phase are employed).

TABLE I
PARAMETERS OF THE MACHINE UNDER TEST

Symbol	Quantity	Unit	Set 1	Set 2	Set 3
p	pole pairs	-		3	
T_{rated}	rated torque	N·m		7.1	
P_{rated}	rated power	kW		1.1	
R_{sk}	stator resistance	Ω	8.2	7.9	8.2
L_{lsk}	stator leakage inductance	mH	18.5	10.3	18.5
M_d , M_q	magnetizing inductances	mH		10.5	
λ_m	PM flux linkage	V·s		0.265	
I_{rated}	rated RMS current	A		1.5	
J_{eq}	mechanical inertia	kg·m^2		0.0133	

(Infineon FS50R12KE3, 50 A, 1200 V), and is fed by a single dc power source at 450 V. The switching frequency has been set at 5 kHz, with hardware-implemented dead-time of 6 µs.

The digital controller has consisted of the dSpace DS1006, using 10 kHz of sampling frequency (double-edge PWM modulation).

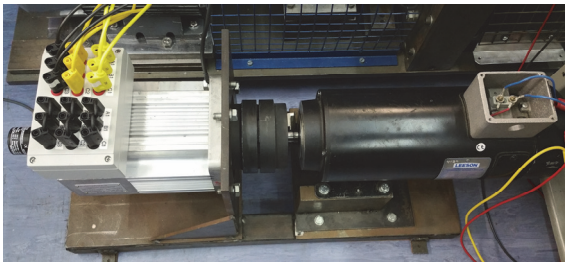

Fig. 12. View of the machine under test (left) and driving machine (right).

B. Experimental Results

The experimental results are provided for the drive operation with both torque and speed control modes. The gains of the units' controllers (PI) have been tuned to achieve a theoretical bandwidth of 600 Hz and a maximum overshoot of 20% when a step reference is applied. In this way, the dynamic performance of the CVCs is demonstrated. Since the machine under test has a surface-mounted distribution of the PMs, the optimal (d,q) currents of the units have been computed using the MTPA relationships reported in (12). Concerning the voltage decoupling algorithm, by applying (15) for each unit, the reference (d,q) voltages have been obtained as:

$$\begin{aligned}
v^*_{s1,d} &= \tilde{K}_{c,d}\cdot\left[\left(1+\tilde{w}_{d,1}\right)\cdot F^*_{1,d}+\tilde{w}_{d,2}\cdot F^*_{2,d}+\tilde{w}_{d,3}\cdot F^*_{3,d}\right]\\
v^*_{s1,q} &= \tilde{K}_{c,q}\cdot\left[\left(1+\tilde{w}_{q,1}\right)\cdot F^*_{1,q}+\tilde{w}_{q,2}\cdot F^*_{2,q}+\tilde{w}_{q,3}\cdot F^*_{3,q}\right]\\
v^*_{s2,d} &= \tilde{K}_{c,d}\cdot\left[\tilde{w}_{d,1}\cdot F^*_{1,d}+\left(1+\tilde{w}_{d,2}\right)\cdot F^*_{2,d}+\tilde{w}_{d,3}\cdot F^*_{3,d}\right]\\
v^*_{s2,q} &= \tilde{K}_{c,q}\cdot\left[\tilde{w}_{q,1}\cdot F^*_{1,q}+\left(1+\tilde{w}_{q,2}\right)\cdot F^*_{2,q}+\tilde{w}_{q,3}\cdot F^*_{3,q}\right]\\
v^*_{s3,d} &= \tilde{K}_{c,d}\cdot\left[\tilde{w}_{d,1}\cdot F^*_{1,d}+\tilde{w}_{d,2}\cdot F^*_{2,d}+\left(1+\tilde{w}_{d,3}\right)\cdot F^*_{3,d}\right]\\
v^*_{s3,q} &= \tilde{K}_{c,q}\cdot\left[\tilde{w}_{q,1}\cdot F^*_{1,q}+\tilde{w}_{q,2}\cdot F^*_{2,q}+\left(1+\tilde{w}_{q,3}\right)\cdot F^*_{3,q}\right]
\end{aligned} \tag{16}$$

where the terms $\tilde{K}_{c,d}$ and $\tilde{K}_{c,q}$ are computed as:

$$\begin{aligned}
\tilde{K}_{c,d} &= \left(1+\tilde{w}_{d,1}+\tilde{w}_{d,2}+\tilde{w}_{d,3}\right)^{-1}\\
\tilde{K}_{c,q} &= \left(1+\tilde{w}_{q,1}+\tilde{w}_{q,2}+\tilde{w}_{q,3}\right)^{-1}
\end{aligned} \tag{17}$$

while the coupling coefficients (5), (6) correspond to:

$$\begin{aligned}
\tilde{w}_{d,1} &= \frac{\tilde{M}_d}{\tilde{L}_{ls1}}\cdot x_{f,1}\ ,\ \tilde{w}_{d,2}=\frac{\tilde{M}_d}{\tilde{L}_{ls2}}\cdot x_{f,2}\ ,\ \tilde{w}_{d,3}=\frac{\tilde{M}_d}{\tilde{L}_{ls3}}\cdot x_{f,3}\\
\tilde{w}_{q,1} &= \frac{\tilde{M}_q}{\tilde{L}_{ls1}}\cdot x_{f,1}\ ,\ \tilde{w}_{q,2}=\frac{\tilde{M}_q}{\tilde{L}_{ls2}}\cdot x_{f,2}\ ,\ \tilde{w}_{q,3}=\frac{\tilde{M}_q}{\tilde{L}_{ls3}}\cdot x_{f,3}
\end{aligned} \tag{18}$$

Since the machine under test is a surface-mounted PMSM, for each set, the d-axis coupling coefficients (5) are identical to those of the q-axis (6).

1) Torque control mode

The open-loop torque control has been tested with the dc machine acting as the prime mover (speed-controlled). The mechanical speed has been set at 1500 rpm. The balanced operation of the units has been imposed ($t_{d,k}^*=t_{q,k}^*=1$, $k=1\div3$). The overall reference torque T^* has been suddenly changed from -12.5 Nm to 12.5 Nm, corresponding to 175% of the machine rated torque. The results are shown in Fig. 13. The fast and well-controlled torque response is noted. Since the second set has a leakage inductance lower than the other two (Table I), it is noted how its q-axis current (torque) has reached first the reference. Besides, the subsequent clamping action, performed by the q-axis controller to keep the current at the reference value, is to be noted. Therefore, this test demonstrates how the modular CVC scheme achieves a decoupled control of each unit, even when the stator sets have different parameters.

2) Speed control mode

The closed-loop speed control has been tested with the dc machine acting as a mechanical load (torque-controlled), while the tested nine-phase machine was speed-controlled. The theoretical bandwidth of the speed loop has been set at 20 Hz. Like in the previous test, the balanced operation of the units has been imposed. The experimental results for a sequence of reference speed steps (0 rpm→ 1500 rpm → -1500 rpm → 0 rpm) are shown in Figs. 14-15.

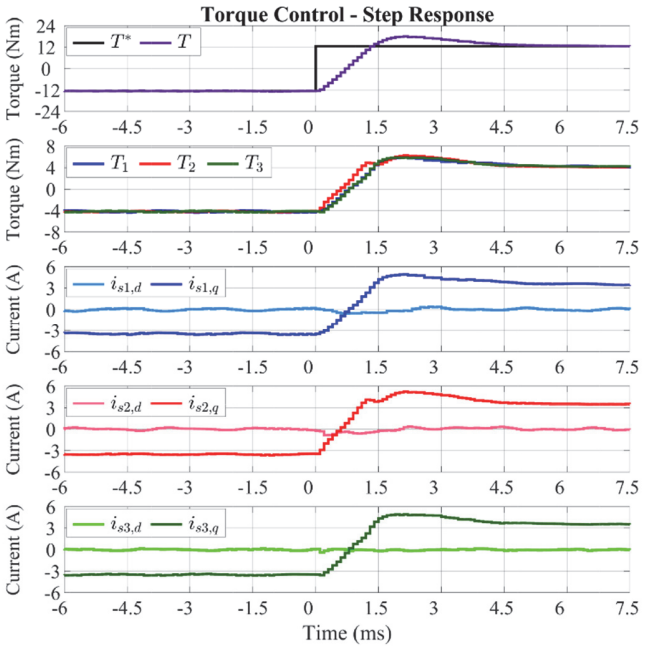

Fig. 13. Torque step response from 175% rated torque in generation to 175% rated torque in motoring at 1500 r/m.

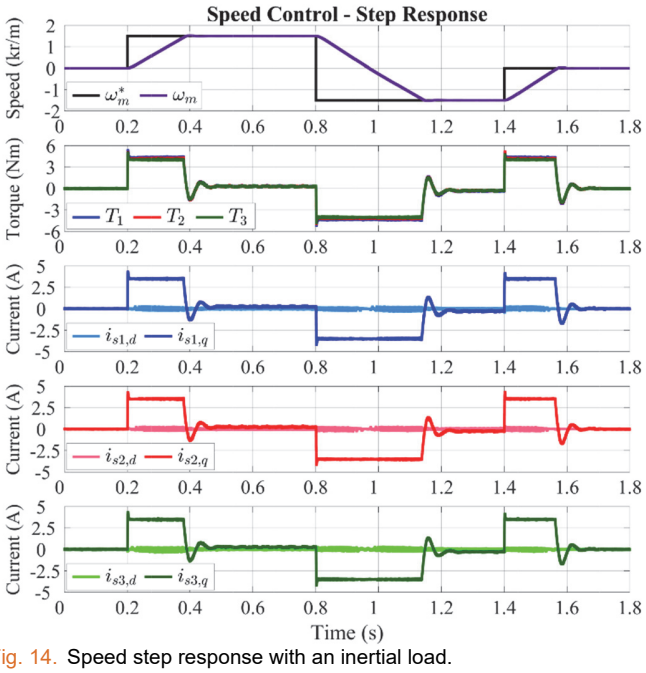

Fig. 14. Speed step response with an inertial load.

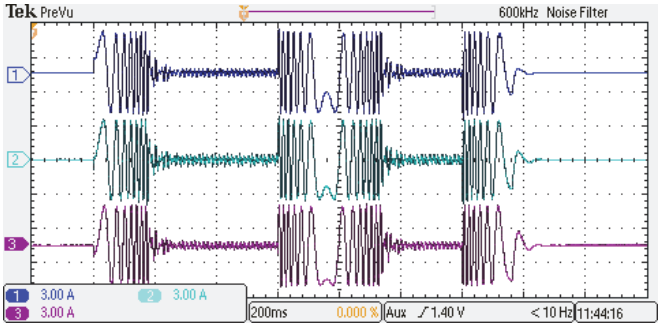

Fig. 15. Speed step response with an inertial load. Ch1: $i_{s1,a}$ (3 A/div), Ch2: $i_{s2,a}$ (3 A/div), Ch3: $i_{s3,a}$ (3 A/div). Time scale: 200 ms/div.

The dc machine has been turned off emulating an inertial load. The very good speed response can be observed, together with the independent and dynamic control of the torque produced by every single set.

In the following, the dc machine has been controlled as a dynamic load. In this way, the load-rejection of the closed-loop speed control has been tested. The results are shown in Fig. 16. A load torque of 12 Nm has suddenly been applied, starting from the no-load condition at 1500 rpm. The speed controller has immediately increased the torque demand to the three sets in a modular way. It is evident that the torque/current response of each set is well controlled. Subsequently, the load torque has suddenly been reversed from 12 Nm to -12 Nm, switching the operation of the machine under test from the motoring to generation. Again, the torque reversal has happened in a modular way among the sets. Besides, it is noted how the q-axis current of each set has adequately been limited to respect the machine current limit ($I_{sk,max}$ = 3.5 A, k=1÷3).

3) Torque-sharing operation

The torque-sharing operation among the units has been tested in closed-loop speed control mode. A total constant load torque of 5 Nm has been applied. Therefore, for each unit, a base reference torque of 1.67 Nm has been set. However, each q-axis torque-sharing coefficient (13) has been deliberately defined to produce a torque oscillation with an amplitude of 1.67 Nm and a frequency of 10 Hz. The torque oscillations of the units have also been shifted from each other in time, emulating a three-phase system. In this way, the units' torques have always been kept different from each other, although their sum is constant (5 Nm). The experimental results are shown in Figs. 17-18.

Finally, unit 2 has been suddenly turned off, emulating an open-winding fault event. The "fault ride-through" capability of the drive can be seen. Indeed, the base torque of the units has been increased at 2.5 Nm, keeping constant the machine torque. Concerning the torque-sharing coefficients, they have been changed to produce torque oscillations of 2.5 Nm that are out-of phase to get a total mean torque of 5 Nm.

It is noted how the currents of the healthy units have been controlled without issues. Therefore, the torque-sharing capability of the proposed scheme in both healthy and faulty conditions has been fully demonstrated. Concerning the voltage decoupling algorithm (15), since unit 2 has been turned off ($x_{f,2} = w_{d,2} = w_{q,2} = 0$), the reference ($d$,$q$) voltages of the healthy units 1 and 3 have simply been computed as:

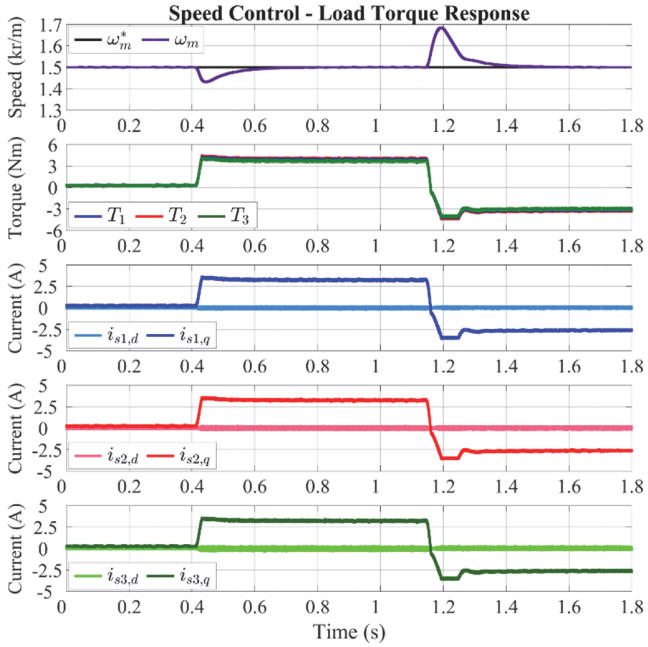

Fig. 16. Load-rejection response at 1500 rpm.

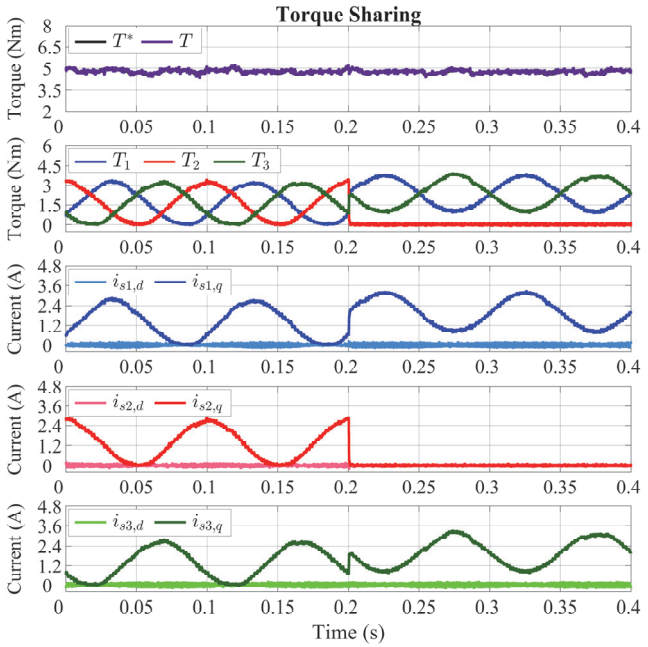

Fig. 17. Torque sharing performance with unit 2 shut-off.

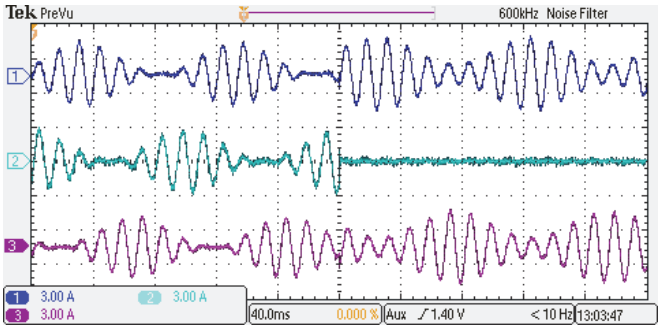

Fig. 18. Torque sharing performance with unit 2 shut-off. Ch1: $i_{s1,a}$ (3 A/div), Ch2: $i_{s2,a}$ (3 A/div), Ch3: $i_{s3,a}$ (3 A/div). Time scale: 40 ms/div.

$$
\begin{aligned}
v^*_{s1,d} &= \left(1+\tilde{w}_{d,1}+\tilde{w}_{d,3}\right)^{-1}\cdot\left[\left(1+\tilde{w}_{d,1}\right)\cdot F^*_{1,d}+\tilde{w}_{d,3}\cdot F^*_{3,d}\right]\\
v^*_{s1,q} &= \left(1+\tilde{w}_{q,1}+\tilde{w}_{q,3}\right)^{-1}\cdot\left[\left(1+\tilde{w}_{q,1}\right)\cdot F^*_{1,q}+\tilde{w}_{q,3}\cdot F^*_{3,q}\right]\\
v^*_{s3,d} &= \left(1+\tilde{w}_{d,1}+\tilde{w}_{d,3}\right)^{-1}\cdot\left[\tilde{w}_{d,1}\cdot F^*_{1,d}+\left(1+\tilde{w}_{d,3}\right)\cdot F^*_{3,d}\right]\\
v^*_{s3,q} &= \left(1+\tilde{w}_{q,1}+\tilde{w}_{q,3}\right)^{-1}\cdot\left[\tilde{w}_{q,1}\cdot F^*_{1,q}+\left(1+\tilde{w}_{q,3}\right)\cdot F^*_{3,q}\right]
\end{aligned}
\tag{19}
$$

It is noted how, thanks to the definition of the coefficients (5)-(6), the voltage decoupling algorithm (15) after an open-phase fault event is straightforward to formulate, as it is just necessary to set to zero the logic states ($x_{f,k}$) of the faulty units.

V. Conclusion

The article proposes a modular vector control scheme for multi-three-phase permanent magnet synchronous machines. The modularity is intended at torque control level and can be extended at digital controller level if a multi-core microcontroller is employed.

The proposed solution yields the highest degree of modularity of the electric drive. Besides, it can deal with atypical multi-three-phase configurations (adopted for cost reasons) for which the application of the vector space decomposition approach has not been presented yet. The performance of the proposed control has been validated with a nine-phase prototype. The experimental results demonstrate the feasibility of the proposed control scheme both in healthy and faulty operation (open-winding fault events), as well as the torque-sharing capability. The advantages of the proposed solution can be summarized as follows:

1) Decoupled control of the currents of each three-phase set, allowing the high performance of the torque regulation.
2) The method can deal with atypical stator winding configurations that can result due to the use of off-the-shelf stator cores, reducing cost and design times.

Appendix: Details of the Model Derivation

In the following, the mathematical manipulations for computing the state-space model (7) of a generic set k (k=1÷n) and the voltage decoupling equations (15), are reported.

1) State-space model of a generic set k (k = 1÷n)

The magnetic models (3) of two generic sets k and z (k=1÷n, z=1÷n, $k \neq z$) are considered:

$$
\bar{\lambda}_{sk,dq} = L_{lsk}\cdot\bar{i}_{sk,dq}+\begin{bmatrix}M_d & 0\\ 0 & M_q\end{bmatrix}\cdot\sum_{u=1}^{n}\bar{i}_{su,dq}+\begin{bmatrix}\lambda_m\\ 0\end{bmatrix} \tag{20}
$$

$$
\bar{\lambda}_{sz,dq} = L_{lsz}\cdot\bar{i}_{sz,dq}+\begin{bmatrix}M_d & 0\\ 0 & M_q\end{bmatrix}\cdot\sum_{u=1}^{n}\bar{i}_{su,dq}+\begin{bmatrix}\lambda_m\\ 0\end{bmatrix} \tag{21}
$$

where the summation index of (3) has been formally changed from z to u, to avoid confusion. By combining (20) and (21), the following equations are obtained:

$$
\bar{\lambda}_{sz,dq}-\bar{\lambda}_{sk,dq} = L_{lsz}\cdot\bar{i}_{sz,dq}-L_{lsk}\cdot\bar{i}_{sk,dq} \tag{22}
$$

$$
\bar{i}_{sz,dq} = \frac{1}{L_{lsz}}\cdot\left(\bar{\lambda}_{sz,dq}-\bar{\lambda}_{sk,dq}+L_{lsk}\cdot\bar{i}_{sk,dq}\right) \tag{23}
$$

Using (23), the time-derivative of the z-set current vector is expressed next as:

$$
\frac{d}{dt}\bar{i}_{sz,dq} = \frac{1}{L_{lsz}}\cdot\left(\frac{d}{dt}\bar{\lambda}_{sz,dq}-\frac{d}{dt}\bar{\lambda}_{sk,dq}+L_{lsk}\cdot\frac{d}{dt}\bar{i}_{sk,dq}\right) \tag{24}
$$

The electric models (2) of two generic sets k and z (k=1÷n, z=1÷n, $k \neq z$) are considered:

$$
\bar{v}_{sk,dq} = R_{sk}\cdot\bar{i}_{sk,dq}+\frac{d}{dt}\bar{\lambda}_{sk,dq}+J\cdot\omega_r\cdot\bar{\lambda}_{sk,dq} \tag{25}
$$

$$
\bar{v}_{sz,dq} = R_{sz}\cdot\bar{i}_{sz,dq}+\frac{d}{dt}\bar{\lambda}_{sz,dq}+J\cdot\omega_r\cdot\bar{\lambda}_{sz,dq} \tag{26}
$$

By combining (25) and (26), the following is obtained:

$$
\begin{aligned}
&\frac{d}{dt}\bar{\lambda}_{sz,dq}-\frac{d}{dt}\bar{\lambda}_{sk,dq} = \left(\bar{v}_{sz,dq}-\bar{v}_{sk,dq}\right)+\ldots\\
&-\left(R_{sz}\cdot\bar{i}_{sz,dq}-R_{sk}\cdot\bar{i}_{sk,dq}\right)-J\cdot\omega_r\cdot\left(\bar{\lambda}_{sz,dq}-\bar{\lambda}_{sk,dq}\right)
\end{aligned}
\tag{27}
$$

Substituting (22) into (27) yields:

$$
\begin{aligned}
&\frac{d}{dt}\bar{\lambda}_{sz,dq}-\frac{d}{dt}\bar{\lambda}_{sk,dq} = \left(\bar{v}_{sz,dq}-\bar{v}_{sk,dq}\right)+\ldots\\
&-\left(R_{sz}\cdot\bar{i}_{sz,dq}-R_{sk}\cdot\bar{i}_{sk,dq}\right)-J\cdot\omega_r\cdot\left(L_{lsz}\cdot\bar{i}_{sz,dq}-L_{lsk}\cdot\bar{i}_{sk,dq}\right)
\end{aligned}
\tag{28}
$$

By inserting (28) into (24), the time-derivative of the z-set current vector can be expressed as a function of the time-derivative of the k-set current vector only:

$$
\begin{aligned}
&\frac{d}{dt}\bar{i}_{sz,dq} = \frac{L_{lsk}}{L_{lsz}}\cdot\frac{d}{dt}\bar{i}_{sk,dq}+\ldots\\
&\ldots-L_{lsz}^{-1}\cdot\left(\bar{v}_{sk,dq}-R_{sk}\cdot\bar{i}_{sk,dq}-J\cdot\omega_r\cdot L_{lsk}\cdot\bar{i}_{sk,dq}\right)+\ldots\\
&\ldots+L_{lsz}^{-1}\cdot\left(\bar{v}_{sz,dq}-R_{sz}\cdot\bar{i}_{sz,dq}-J\cdot\omega_r\cdot L_{lsz}\cdot\bar{i}_{sz,dq}\right)
\end{aligned}
\tag{29}
$$

For the reasons that will become obvious later, the following expression is computed from (29):

$$
\begin{aligned}
&\sum_{z=1,z\neq k}^{n}\left(\frac{d}{dt}\bar{i}_{sz,dq}\right) = L_{lsk}\cdot\frac{d}{dt}\bar{i}_{sk,dq}\cdot\sum_{z=1,z\neq k}^{n}L_{lsz}^{-1}+\ldots\\
&\ldots-\left(\bar{v}_{sk,dq}-R_{sk}\cdot\bar{i}_{sk,dq}-J\cdot\omega_r\cdot L_{lsk}\cdot\bar{i}_{sk,dq}\right)\cdot\sum_{z=1,z\neq k}^{n}L_{lsz}^{-1}+\ldots\\
&\ldots+\sum_{z=1,z\neq k}^{n}\left[L_{lsz}^{-1}\cdot\left(\bar{v}_{sz,dq}-R_{sz}\cdot\bar{i}_{sz,dq}-J\cdot\omega_r\cdot L_{lsz}\cdot\bar{i}_{sz,dq}\right)\right]
\end{aligned}
\tag{30}
$$

and is then resolved along the (d,q) axes into:

$$
\begin{aligned}
&\sum_{z=1,z\neq k}^{n}\left(\frac{d}{dt}i_{sz,d}\right) = L_{lsk}\cdot\frac{d}{dt}i_{sk,d}\cdot\sum_{z=1,z\neq k}^{n}L_{lsz}^{-1}+\ldots\\
&\ldots-\left(v_{sk,d}-R_{sk}\cdot i_{sk,d}+\omega_r\cdot L_{lsk}\cdot i_{sk,q}\right)\cdot\sum_{z=1,z\neq k}^{n}L_{lsz}^{-1}+\ldots\\
&\ldots+\sum_{z=1,z\neq k}^{n}\left[L_{lsz}^{-1}\cdot\left(v_{sz,d}-R_{sz}\cdot i_{sz,d}+\omega_r\cdot L_{lsz}\cdot i_{sz,q}\right)\right]
\end{aligned}
\tag{31}
$$

$$
\begin{aligned}
&\sum_{z=1,z\neq k}^{n}\left(\frac{d}{dt}i_{sz,q}\right) = L_{lsk}\cdot\frac{d}{dt}i_{sk,q}\cdot\sum_{z=1,z\neq k}^{n}L_{lsz}^{-1}+\ldots\\
&\ldots-\left(v_{sk,q}-R_{sk}\cdot i_{sk,q}-\omega_r\cdot L_{lsk}\cdot i_{sk,d}\right)\cdot\sum_{z=1,z\neq k}^{n}L_{lsz}^{-1}+\ldots\\
&\ldots+\sum_{z=1,z\neq k}^{n}\left[L_{lsz}^{-1}\cdot\left(v_{sz,q}-R_{sz}\cdot i_{sz,q}-\omega_r\cdot L_{lsz}\cdot i_{sz,d}\right)\right]
\end{aligned}
\tag{32}
$$

The *k*-set magnetic equation (20) is substituted in the *k*-set electric equation (25), leading to the following:

$$\begin{aligned}&\bar{v}_{sk,dq} = R_{sk}\cdot\bar{i}_{sk,dq} + ...\\&...+ L_{lsk}\cdot\frac{d}{dt}\bar{i}_{sk,dq} + \begin{bmatrix} M_d & 0\\ 0 & M_q\end{bmatrix}\cdot\left[\frac{d}{dt}\bar{i}_{sk,dq} + \sum_{\substack{u=1\\u\neq k}}^{n}\left(\frac{d}{dt}\bar{i}_{su,dq}\right)\right] + ...\\&...+ J\cdot\omega_r\cdot L_{lsk}\cdot\bar{i}_{sk,dq} + J\cdot\omega_r\cdot\begin{bmatrix} M_d & 0\\ 0 & M_q\end{bmatrix}\cdot\left[\bar{i}_{sk,dq} + \sum_{\substack{u=1\\u\neq k}}^{n}\bar{i}_{su,dq}\right] + ...\\&...+ J\cdot\omega_r\cdot\begin{bmatrix}\lambda_m\\ 0\end{bmatrix}\end{aligned} \tag{33}$$

Next, by resolving (33) along the (*d*,*q*) axes, and by formally changing the summation index from *u* to *z*, the following is obtained:

$$\begin{aligned}&v_{sk,d} = R_{sk}\cdot i_{sk,d} + \left(L_{lsk}+M_d\right)\cdot\frac{d}{dt}i_{sk,d} + M_d\cdot\sum_{z=1,z\neq k}^{n}\left(\frac{d}{dt}i_{sz,d}\right) + ...\\&...-\omega_r\cdot\left(L_{lsk}+M_q\right)\cdot i_{sk,q} - \omega_r\cdot M_q\cdot\sum_{z=1,z\neq k}^{n} i_{sz,q}\end{aligned} \tag{34}$$

$$\begin{aligned}&v_{sk,q} = R_{sk}\cdot i_{sk,q} + \left(L_{lsk}+M_q\right)\cdot\frac{d}{dt}i_{sk,q} + M_q\cdot\sum_{z=1,z\neq k}^{n}\left(\frac{d}{dt}i_{sz,q}\right) + ...\\&...+\omega_r\cdot\left(L_{lsk}+M_d\right)\cdot i_{sk,d} + \omega_r\cdot M_d\cdot\sum_{z=1,z\neq k}^{n} i_{sz,d} + \omega_r\cdot\lambda_m\end{aligned} \tag{35}$$

Expressions (31), (32) are further inserted into (34), (35), respectively. Also, by considering that all the machine's sets are active, the coupling coefficients (5), (6) are used to simplify the resulting equations, leading to the following:

$$\begin{aligned}&\left(L_{lsk}+M_d+c_{d,k}\cdot L_{lsk}\right)\cdot\frac{d}{dt}i_{sk,d} = ...\\&...-\left(R_{sk}+c_{d,k}\cdot R_{sk}\right)\cdot i_{sk,d} + \omega_r\cdot\left(c_{d,k}\cdot L_{lsk} + L_{lsk} + M_q\right)\cdot i_{sk,q} + ...\\&...+\sum_{z=1,z\neq k}^{n}\left[\left(w_{d,z}\cdot R_{sz}\right)\cdot i_{sz,d} + \omega_r\cdot\left(M_q - M_d\right)\cdot i_{sz,q}\right] + ...\\&...+\left(1+c_{d,k}\right)\cdot v_{sk,d} - \sum_{z=1,z\neq k}^{n}\left(w_{d,z}\cdot v_{sz,d}\right)\end{aligned} \tag{36}$$

$$\begin{aligned}&\left(L_{lsk}+M_q+c_{q,k}\cdot L_{lsk}\right)\cdot\frac{d}{dt}i_{sk,q} = ...\\&...-\omega_r\cdot\left(c_{q,k}\cdot L_{lsk} + L_{lsk} + M_d\right)\cdot i_{sk,d} - \left(R_{sk}+c_{q,k}\cdot R_{sk}\right)\cdot i_{sk,q} + ...\\&...+\sum_{z=1,z\neq k}^{n}\left[\omega_r\cdot\left(M_q - M_d\right)\cdot i_{sz,d} + \left(w_{q,z}\cdot R_{sz}\right)\cdot i_{sz,q}\right] + ...\\&...+\omega_r\cdot\lambda_m + \left(1+c_{q,k}\right)\cdot v_{sk,q} - \sum_{z=1,z\neq k}^{n}\left(w_{q,z}\cdot v_{sz,q}\right)\end{aligned} \tag{37}$$

Finally, using parameters and variables defined in (8)-(11) in the formulation of (36), (37), the following is obtained:

$$\begin{cases}L_{d,k}\cdot\dfrac{d}{dt}i_{sk,d} = X_{dd,k}\cdot i_{sk,d} + X_{dq,k}\cdot i_{sk,q} + ...\\\quad ...+\displaystyle\sum_{z=1,z\neq k}^{n}\left(Y_{dd,z}\cdot i_{sz,d} + Y_{dq,z}\cdot i_{sz,q}\right) + F_{k,d}\\L_{q,k}\cdot\dfrac{d}{dt}i_{sk,q} = X_{qd,k}\cdot i_{sk,d} + X_{qq,k}\cdot i_{sk,q} + ...\\\quad ...+\displaystyle\sum_{z=1,z\neq k}^{n}\left(Y_{qd,z}\cdot i_{sz,d} + Y_{qq,z}\cdot i_{sz,q}\right) - \omega_r\cdot\lambda_m + F_{k,q}\end{cases} \tag{38}$$

The (*d*,*q*) equations of (38) correspond to the space-state model associated with the generic set *k* (*k*=1÷*n*), given in (7). Hence the proof of correctness of (7) is completed.

2) Voltage decoupling equation

According to (14), outputs of each CVC scheme correspond to the specific reference combinations ($F_{k,d}^*$, $F_{k,q}^*$) of the (*d*,*q*) voltages belonging to all units. Therefore, by merging (14) for all units, the following is obtained:

$$\begin{bmatrix}F_{1,d}^*\\F_{2,d}^*\\...\\F_{k,d}^*\\...\\F_{n,d}^*\end{bmatrix} = \begin{bmatrix}c_{d,1} & w_{d,2} & ... & w_{d,k} & ... & w_{d,n}\\ w_{d,1} & c_{d,2} & ... & w_{d,k} & ... & w_{d,n}\\ ... & ... & ... & ... & ... & ...\\ w_{d,1} & w_{d,2} & ... & c_{d,k} & ... & w_{d,n}\\ ... & ... & ... & ... & ... & ...\\ w_{d,1} & w_{d,2} & ... & w_{d,k} & ... & c_{d,n}\end{bmatrix}\cdot\begin{bmatrix}v_{s1,d}^*\\v_{s2,d}^*\\...\\v_{sk,d}^*\\...\\v_{sn,d}^*\end{bmatrix} = \left[C_d\right]\cdot\begin{bmatrix}v_{s1,d}^*\\v_{s2,d}^*\\...\\v_{sk,d}^*\\...\\v_{sn,d}^*\end{bmatrix} \tag{39}$$

$$\begin{bmatrix}F_{1,q}^*\\F_{2,q}^*\\...\\F_{k,q}^*\\...\\F_{n,q}^*\end{bmatrix} = \begin{bmatrix}c_{q,1} & w_{q,2} & ... & w_{q,k} & ... & w_{q,n}\\ w_{q,1} & c_{q,2} & ... & w_{q,k} & ... & w_{q,n}\\ ... & ... & ... & ... & ... & ...\\ w_{q,1} & w_{q,2} & ... & c_{q,k} & ... & w_{q,n}\\ ... & ... & ... & ... & ... & ...\\ w_{q,1} & w_{q,2} & ... & w_{q,k} & ... & c_{q,n}\end{bmatrix}\cdot\begin{bmatrix}v_{s1,q}^*\\v_{s2,q}^*\\...\\v_{sk,q}^*\\...\\v_{sn,q}^*\end{bmatrix} = \left[C_q\right]\cdot\begin{bmatrix}v_{s1,q}^*\\v_{s2,q}^*\\...\\v_{sk,q}^*\\...\\v_{sn,q}^*\end{bmatrix} \tag{40}$$

The proposed decoupling algorithm performs the computation of the reference (*d*,*q*) voltages of the units starting from the outputs of all CVC schemes, leading to:

$$\begin{bmatrix}v_{s1,d}^*\\v_{s2,d}^*\\...\\v_{sk,d}^*\\...\\v_{sn,d}^*\end{bmatrix} = \left[C_d\right]^{-1}\cdot\begin{bmatrix}F_{s1,d}^*\\F_{s2,d}^*\\...\\F_{sk,d}^*\\...\\F_{sn,d}^*\end{bmatrix},\quad \begin{bmatrix}v_{s1,q}^*\\v_{s2,q}^*\\...\\v_{sk,q}^*\\...\\v_{sn,q}^*\end{bmatrix} = \left[C_q\right]^{-1}\cdot\begin{bmatrix}F_{s1,q}^*\\F_{s2,q}^*\\...\\F_{sk,q}^*\\...\\F_{sn,q}^*\end{bmatrix} \tag{41}$$

where the inverse matrices $[C_d]^{-1}$ and $[C_q]^{-1}$ are computed as:

$$\left[C_d\right]^{-1} = \frac{1}{1+\sum_{z=1}^{n} w_{d,z}}\cdot\begin{bmatrix}(1+w_{d,1}) & w_{d,2} & ... & w_{d,k} & ... & w_{d,n}\\ w_{d,1} & (1+w_{d,2}) & ... & w_{d,k} & ... & w_{d,n}\\ ... & ... & ... & ... & ... & ...\\ w_{d,1} & w_{d,2} & ... & (1+w_{d,k}) & ... & w_{d,n}\\ ... & ... & ... & ... & ... & ...\\ w_{d,1} & w_{d,2} & ... & w_{d,k} & ... & (1+w_{d,n})\end{bmatrix} \tag{42}$$

$$\left[C_q\right]^{-1}=\frac{1}{1+\sum_{z=1}^{n}w_{q,z}}\cdot\begin{bmatrix}(1+w_{q,1}) & w_{q,2} & \dots & w_{q,k} & \dots & w_{q,n}\\ w_{q,1} & (1+w_{q,2}) & \dots & w_{q,k} & \dots & w_{q,n}\\ \dots & \dots & \dots & \dots & \dots & \dots\\ w_{q,1} & w_{q,2} & \dots & (1+w_{q,k}) & \dots & w_{q,n}\\ \dots & \dots & \dots & \dots & \dots & \dots\\ w_{q,1} & w_{q,2} & \dots & w_{q,k} & \dots & (1+w_{q,n})\end{bmatrix} \tag{43}$$

Therefore, the reference (d,q) voltages of the generic set k (k=1÷n) are computed as:

$$\begin{aligned} v^{*}_{sk,d}&=\left(1+\sum_{z=1}^{n}w_{d,z}\right)^{-1}\cdot\left[F^{*}_{k,d}+\sum_{z=1}^{n}\left(w_{d,z}\cdot F^{*}_{z,d}\right)\right]\\ v^{*}_{sk,q}&=\left(1+\sum_{z=1}^{n}w_{q,z}\right)^{-1}\cdot\left[F^{*}_{k,q}+\sum_{z=1}^{n}\left(w_{q,z}\cdot F^{*}_{z,q}\right)\right]\end{aligned} \tag{44}$$

thus proving the voltage decoupling equations given in (15).

REFERENCES

[1] 'Ertrac - Welcome'. https://www.ertrac.org/ (accessed Mar. 19, 2020).

[2] E. Levi, 'Multiphase Electric Machines for Variable-Speed Applications', *IEEE Trans. Ind. Electron.*, vol. 55, no. 5, pp. 1893–1909, May 2008.

[3] F. Barrero and M. J. Duran, 'Recent Advances in the Design, Modeling, and Control of Multiphase Machines—Part I', *IEEE Trans. Ind. Electron.*, vol. 63, no. 1, pp. 449–458, Jan. 2016.

[4] M. J. Duran and F. Barrero, 'Recent Advances in the Design, Modeling, and Control of Multiphase Machines—Part II', *IEEE Trans. Ind. Electron.*, vol. 63, no. 1, pp. 459–468, Jan. 2016.

[5] A. Tessarolo, G. Zocco, and C. Tonello, 'Design and Testing of a 45-MW 100-Hz Quadruple-Star Synchronous Motor for a Liquefied Natural Gas Turbo-Compressor Drive', *IEEE Trans. Ind. Appl.*, vol. 47, no. 3, pp. 1210–1219, May 2011.

[6] R. Bojoi, S. Rubino, A. Tenconi, and S. Vaschetto, 'Multiphase electrical machines and drives: A viable solution for energy generation and transportation electrification', in *2016 EPE*, 2016, pp. 632–639.

[7] W. Cao, B. C. Mecrow, G. J. Atkinson, J. W. Bennett, and D. J. Atkinson, 'Overview of Electric Motor Technologies Used for More Electric Aircraft (MEA)', *IEEE Trans. Ind. Electron.*, vol. 59, no. 9, pp. 3523–3531, Sep. 2012.

[8] S. Rubino, R. Bojoi, A. Cavagnino, and S. Vaschetto, 'Asymmetrical twelve-phase induction starter/generator for more electric engine in aircraft', in *2016 IEEE Energy Conversion Congress and Exposition (ECCE)*, Sep. 2016, pp. 1–8.

[9] I. Zoric, M. Jones, and E. Levi, 'Arbitrary Power Sharing Among Three-Phase Winding Sets of Multiphase Machines', *IEEE Trans. Ind. Electron.*, vol. 65, no. 2, pp. 1128–1139, Feb. 2018.

[10] Y. Hu, Z. Q. Zhu, and M. Odavic, 'Comparison of Two-Individual Current Control and Vector Space Decomposition Control for Dual Three-Phase PMSM', *IEEE Trans. Ind. Appl.*, vol. 53, no. 5, pp. 4483–4492, Sep. 2017.

[11] R. Bojoi, A. Cavagnino, A. Tenconi, and S. Vaschetto, 'Control of Shaft-Line-Embedded Multiphase Starter/Generator for Aero-Engine', *IEEE Trans. Ind. Electron.*, vol. 63, no. 1, pp. 641–652, Jan. 2016.

[12] A. S. Abdel-Khalik, A. M. Massoud, and S. Ahmed, 'Application of Standard Three-Phase Stator Frames in Prime Phase Order Multiphase Machine Construction', *IEEE Trans. Ind. Electron.*, vol. 66, no. 4, pp. 2506–2517, Apr. 2019.

[13] Y. Zhao and T. A. Lipo, 'Space vector PWM control of dual three-phase induction machine using vector space decomposition', *IEEE Trans. Ind. Appl.*, vol. 31, no. 5, pp. 1100–1109, Sep. 1995.

[14] E. Levi, R. Bojoi, F. Profumo, H. A. Toliyat, and S. Williamson, 'Multiphase induction motor drives - a technology status review', *IET Electr. Power Appl.*, vol. 1, no. 4, pp. 489–516, Jul. 2007.

[15] I. Zoric, M. Jones, and E. Levi, 'Vector space decomposition algorithm for asymmetrical multiphase machines', in *2017 International Symposium on Power Electronics (Ee)*, Oct. 2017, pp. 1–6.

[16] R. H. Nelson and P. C. Krause, 'Induction Machine Analysis for Arbitrary Displacement Between Multiple Winding Sets', *IEEE Trans. Power Appar. Syst.*, vol. PAS-93, no. 3, pp. 841–848, May 1974.

[17] S. Rubino, R. Bojoi, F. Mandrile, and E. Armando, 'Modular Stator Flux and Torque Control of Multiphase Induction Motor Drives', in *2019 IEEE International Electric Machines and Drives Conference (IEMDC)*, San Diego, USA, 2019, pp. 531–538.

[18] A. Galassini, A. Costabeber, M. Degano, C. Gerada, A. Tessarolo, and R. Menis, 'Enhanced Power Sharing Transient With Droop Controllers for Multithree-Phase Synchronous Electrical Machines', *IEEE Trans. Ind. Electron.*, vol. 66, no. 7, pp. 5600–5610, Jul. 2019.

[19] I. Zoric, M. Jones, and E. Levi, 'Arbitrary d–q current sharing in three-phase winding sets of multi-phase machines', *J. Eng.*, vol. 2019, no. 17, pp. 4173–4177, 2019.

[20] H. S. Che, E. Levi, M. Jones, M. J. Duran, W. Hew, and N. A. Rahim, 'Operation of a Six-Phase Induction Machine Using Series-Connected Machine-Side Converters', *IEEE Trans. Ind. Electron.*, vol. 61, no. 1, pp. 164–176, Jan. 2014.

[21] E. Jung, H. Yoo, S. Sul, H. Choi, and Y. Choi, 'A Nine-Phase Permanent-Magnet Motor Drive System for an Ultrahigh-Speed Elevator', *IEEE Trans. Ind. Appl.*, vol. 48, no. 3, pp. 987–995, May 2012.

[22] S. Rubino, R. Bojoi, E. Levi, and O. Dordevic, 'Vector Control of Multiple Three-Phase Permanent Magnet Motor Drives', in *IECON 2018 - 44th Annual Conference of the IEEE Industrial Electronics Society*, Oct. 2018, pp. 5866–5871.

[23] P. Krause, O. Wasynczuk, S. D. Sudhoff, and S. Pekarek, *Analysis of Electric Machinery and Drive Systems*. John Wiley & Sons, 2013.

[24] G. Sala, M. Mengoni, G. Rizzoli, L. Zarri, and A. Tani, 'Decoupled d-q Axes Current Sharing Control of Multi Three-Phase Induction Machines', *IEEE Trans. Ind. Electron.*, vol. 67, no. 9, pp. 7124–7134, Sep. 2020.

[25] S. Rubino, R. Bojoi, S. A. Odhano, and P. Zanchetta, 'Model Predictive Direct Flux Vector Control of Multi-three-Phase Induction Motor Drives', *IEEE Trans. Ind. Appl.*, vol. 54, no. 5, pp. 4394–4404, Sep. 2018.

[26] T. M. Jahns, G. B. Kliman, and T. W. Neumann, 'Interior Permanent-Magnet Synchronous Motors for Adjustable-Speed Drives', *IEEE Trans. Ind. Appl.*, vol. IA-22, no. 4, pp. 738–747, Jul. 1986.

[27] E. Armando, R. I. Bojoi, P. Guglielmi, G. Pellegrino, and M. Pastorelli, 'Experimental Identification of the Magnetic Model of Synchronous Machines', *IEEE Trans. Ind. Appl.*, vol. 49, no. 5, pp. 2116–2125, Sep. 2013.

[28] D. G. Holmes and T. A. Lipo, *Pulse Width Modulation for Power Converters: Principles and Practice*. John Wiley & Sons, 2003.

Sandro Rubino (S'16, M'18) received the M.Sc. and Ph.D. degrees in Electrical Engineering from Politecnico di Torino, Torino, Italy, in 2014 and 2019, respectively. He is currently Assistant Professor with Dipartimento Energia "G. Ferraris," Politecnico di Torino. He serves as a reviewer for some IEEE Transactions and international conferences.

His main research interests include power electronics, modeling, and control of multiphase electrical machines and high-performance ac motor drives.

Obrad Dordevic (S'11, M'13) received his Dipl. Ing. degree in Electronic Engineering from the University of Belgrade, Serbia, in 2008. He joined Liverpool John Moores University in December 2009 as a PhD student. Dr Dordevic received his PhD degree in April 2013 and was appointed as a Lecturer at the Liverpool John Moores University in May 2013. In 2018 he was promoted to a Reader in Power Electronics.

His main research interests are in the areas of power electronics, electrostatic precipitators, and advanced variable speed multiphase drive systems.

Iustin Radu Bojoi (SM'10, F'19) received the MSc degree in Electrical Engineering from Technical University of Iasi, Romania, in 1993, and the Ph.D. in Electrical Engineering from Politecnico di Torino, Italy, in 2002. He is a Full Professor of Power Electronics and Electrical Drives in the Energy Department "G. Ferraris" and Chairman of the Power Electronics Innovation Center at Politecnico di Torino, Italy.
Dr. Bojoi published more than 150 papers covering electrical drives and power electronics for industrial applications, transportation electrification, power quality, and home appliances. He was involved in many research projects with industry for direct technology transfer aiming at obtaining new products.
Dr. Bojoi is the co-recipient of 5 prize paper awards, the last one in 2015 as IEEE-IAS Prize Paper Award. Dr. Bojoi is a Co-Editor-In-Chief of the IEEE Transactions on Industrial Electronics and Chair of the Electrical Machines Technical Committee of the Industrial Electronics Society.

Emil Levi (S'89, M'92, SM'99, F'09) received his MSc and the PhD degrees in Electrical Engineering from the University of Belgrade, Yugoslavia in 1986 and 1990, respectively. He joined Liverpool John Moores University, UK in May 1992 and is since September 2000 Professor of Electric Machines and Drives. He served as a Co-Editor-in-Chief of the IEEE Trans. on Industrial Electronics in the 2009-2013 period.
Currently he is Editor-in-Chief of the IEEE Trans. on Industrial Electronics, Editor-in-Chief of the IET Electric Power Applications and an Editor of the IEEE Trans. on Energy Conversion.
He is the recipient of the Cyril Veinott award of the IEEE Power and Energy Society for 2009 and the Best Paper award of the IEEE Trans. on Industrial Electronics for 2008. In 2014 he received the "Outstanding Achievement Award" from the European Power Electronics (EPE) Association and in 2018 the "Professor Istvan Nagy Award" from the Power Electronics and Motion Control (PEMC) Council.